HHS Public Access

Author manuscript

Biochimie. Author manuscript; available in PMC 2017 November 01.

Published in final edited form as:

Biochimie. 2016 November ; 130: 63–75. doi:10.1016/j.biochi.2016.07.012.

Complete structural characterization of ceramides as $[M - H]^-$ ions by multiple-stage linear ion trap mass spectrometry

Fong-Fu Hsu[1,*]

[1]Mass Spectrometry Resource, Division of Endocrinology, Diabetes, Metabolism, and Lipid Research, Department of Internal Medicine, Washington University School of Medicine, St. Louis, MO 63110

Abstract

Ceramide is a huge lipid family consisting of diversified structures including various modifications in the fatty acyl chain and the long chain base (LCB). In this contribution, negative-ion ESI linear ion-trap multiple-stage mass spectrometric method (LIT MS^n) towards complete structural determination of ceramides in ten major families characterized as the $[M - H]^-$ ions is described. Multiple sets of fragment ions reflecting the fatty acyl chain and LCB were observed in the CID MS^2 spectrum, while the sequential MS^3 and MS^4 spectra contain structural information for locating the double bond and the functional groups, permitting realization of the fragmentation processes. Thereby, differentiation of ceramide molecules varied by chain length, the LCB (sphingosine, phytosphigosine, 6-hydroxy-sphingosine), and by the modification (α-hydroxy-, β-hydroxy-, ω-hydroxy-FA) can be achieved; and many isomeric structures in the biological specimen can be revealed in detail.

Keywords

ceramide; tandem mass spectrometry; linear ion-trap; lipidomics; electrospray ionization

1. Introduction

Ceramides are ubiquitous and are one of the major lipids in the lipid bilayer. They are involved in many important physiological processes including apoptosis, differentiation, migration, adhesion, immune responses and cell senescence [1-6]. In the epidermis, ceramides (Cer) comprise the major constituent of sphingolipids and are known to play diverse roles in the outermost layers of the skin function such as water retention and provision of a physical barrier [7-10].

*To whom the correspondence should be addressed: Dr. Fong-Fu Hsu, Box 8127, Washington University School of Medicine, 660 S Euclid, St. Louis, MO 63110. Tel: 314-362-0056, fhsu@im.wustl.edu.

Ceramides consist of a long-chain aliphatic amino alcohol referred to long-chain base (LCB), to which a fatty acyl chain is attached via an amide linkage. They are huge family comprising diversified structures, varied by the chain length, the location and number of unsaturated bond, as well as by the modification such as the presence of hydroxyl group on the LCB and the fatty acyl substituents. Thus, heroic efforts have been attempted for structural characterization of this lipid family. Among them, mass spectrometric approaches, including GC/MS [11, 12], high energy FAB MS/MS [13, 14], and more recently, low energy ESI tandem mass spectrometry with or without online HPLC [15-23] have been reported.

Ceramides are readily detectable by ESI-MS in both positive-ion and negative-ion modes. In the positive-ion mode, ceramides are desorbed as $[M + H]^+$ and $[M + H – H_2O]^+$ ions simultaneously, and ions in the form of $[M + Alk]^+$ (Alk = Li, Na) are also seen, dependent on the presence of Alk^+ when ionization takes place [15-22]. In the negative-ion mode, ceramides form $[M - H]^–$ and $[M + X]^–$ (X = Cl, $RCO_2^–$) ions. The $[M + RCO_2]^–$ adduct ion can be formed with $HCO_2^–$, $CH_3CO_2^–$ [16, 21], as well as with long chain palmitate ($C_{15}H_{31}CO_2^–$) and oleate ($C_{17}H_{33}CO_2^–$) (personal observation).

CID tandem mass spectrometry on the $[M + H]^+$ and $[M + Li]^+$ ions in the positive ion modes, applying FAB-tandem sector [13, 14], ESI-tandem quadrupole and Q-TOF [15, 17, 21, 22], as well as on the [M – H[$^–$ ions in the negative ion mode applied FAB-tandem sector [13, 14], ESI-ITMS [24, 25], and ESI-tandem quadrupole [16, 19] have been used to identify both fatty acyl and LCB substituents of the molecules, and CID tandem mass spectrometry on the $[M + X]^–$ ions (X = Cl, RCO_2) yielded insufficient data for structure characterization [16]. None of the above mentioned methods permits complete structural characterization. In contrast, LIT MS^n on the $[M – H]^–$ ions of all 10 ceramide subfamilies (Scheme 1) included in this study yielded complete information that results in the location of the double bond and the hydroxyl groups of the molecule. The MS^n (n >3) feature readily available for a LIT instrument also affords further insight the fragmentation processes, leading to unveil the complex structures in the biological specimen that contains many isomers.

2. Materials and Methods

2.1. Mass spectrometry

Both high-resolution (R=100,000 at *m/z* 400) and low-energy CID tandem mass spectrometric experiments were conducted on a Thermo Scientific (San Jose, CA) LTQ Orbitrap Velos mass spectrometer (MS) with Xcalibur operating system. To form exclusive $[M - H]^–$ ions, ceramides were dissolved in 1% NH_4OH in methanol and infused (1.5 μL/min) onto the ESI source, where the skimmer was set at ground potential, the electrospray needle was set at 4.0 kV, and temperature of the heated capillary was 300°C. The automatic gain control of the ion trap was set to $5×10^4$, with a maximum injection time of 50 ms. Helium was used as the buffer and collision gas at a pressure of $1×10^{–3}$ mbar (0.75 mTorr). The MS^n experiments were carried out with an optimized relative collision energy ranging from 25-45% and with an activation q value at 0.25, and the activation time at 10 ms to leave a minimal residual precursor ion with abundance around 20%. The mass selection window for the precursor ions was set at 1 Da wide to admit the monoisotopic ion to the ion-trap for

collision-induced dissociation (CID) for unit resolution detection in the ion-trap or high resolution accurate mass detection in the Orbitrap mass analyzer. Mass spectra were accumulated in the profile mode, typically for 2-10 min for MS^n spectra (n=2,3,4).

2.2 Ceramide Standards and Nomenclature

Ceramide standards of d18:1/24:1 and d18:1/18:1 were purchased from Avanti Polar Lipids Inc. (Alabaster, Al); and the rest of others were prepared as described [26-28]. The designations and abbreviations recommended by IUPAC (http://www.chem.qmul.ac.uk/iupac/lipid/) were used. The designation of ceramide is in the form of d(or t)LCB/FA, with d denoting a dihydroxy and t denoting a trihydroxy long chain base (LCB), and FA refers to fatty acid. The sphingosine (sphing-4-enine) and sphinganine LCBs, for examples, are designated as d18:1, and d18:0, respectively. Fatty acyl moieties with or without hydroxyl substituent were denoted as hFA or nFA, respectively; while sphingosine ceramides with α-, β-, or ω-hydroxyl fatty acyl substituent was designated as d18:1/αhFA-Cer, d18:1/βhFA-Cer, d18:1/ωhFA-Cer, respectively. Therefore, N-α-, N-β-, and N-ω-hydroxy-palmitoyl-sphingosine, for example, are designated as d18:1/αh16:0-Cer, d18:1/βh16:0-Cer, d18:1/ωh16:0-Cer, respectively. The nomenclature of Motta et al [29], expanded by Robson et al [30] and Masukawa et al [20] is used for abbreviation of ceramide subfamily (Table 1). The designation of the fragment ions is according to those previously published [16]. In short, fragment ions arising from losses of water, HCHO, and of [H_2O + HCHO] are **common** ions seen for ceramides, and are designated as “c” ions. Thus, ions such as $[M - H - H_2O]^-$, $[M - H - HCHO]^-$, $[M - H - H_2 - HCHO]^-$, $[M - H - 2H_2O]^-$, and $[M - H - H_2O - HCHO]^-$ (in the *m/z* descending order) are designated as c1, c2, c3, c4, and c5 respectively. Fragment ions possessing fatty **acyl** chain structure are designated as “a” ions; while ions bearing the structural information of long chain **base** are designated as “b” ions. Therefore, N-acylethanolamine (NAE) anion ($[NAE - H]^-$) and $[(NAE - H) - H_2]^-$ ions that carry structural information of fatty acyl chain are designated as a1, and a2 ($[a1 - H_2]$) ions respectively. Fragment ions such as $[LCB - H]^-$ and $[LCB - H - HCHO]^-$ that related to the LCB structure are designated as b1, and b2 ions, respectively (Table 1).

3. Results and Discussion

3.1 Complete structural characterization of N-acyl sphingosine (d18:1/nFA-Cer) (Cer[NS] with unsaturated fatty acyl substituent

Complete structural characterization of ceramides containing double bond in the fatty acyl chain is exemplified by the $[M - H]^-$ ions of N-nervonoyl-D-*erythro*-sphingosine (d18:1/24:1-Cer) at m/z 646, which yielded the MS^2 spectrum (Figure 1a) consisting of the common ions at *m/z* 628 (646 - H_2O) (c1), 616 (646 - HCHO) (c2), 614 (646 – [H_2 + HCHO]) (c3), and 598 (646 – H_2O - HCHO) (c4) similar to those obtained with a tandem quadrupole instrument [16]. However, these ions are more prominent, consistent with the notion that collision activated dissociation in an ion-trap is a resonance excitation process in which the consecutive fragmentation processes are minimal. The spectrum (Figure 1a) also contained the predominant ions of *m/z* 406 (a2) and 390 (a3) and ions of *m/z* 365 (RCO_2^-), 364 ($RCONH^-$), 347 ((RCO_2^- - H_2O) that identified the 24:1-fatty acyl chain, along with

the ions of *m/z* 237 (b4), 263 (b5) that recognized the d18:1-LCB (Table 1), giving assignment of the d18:1/24:1-Cer structure [16].

The ion of *m/z* 365(a6) corresponds to the 24:1-FA anion (RCO_2^-). The origin of the ion may derive from the initial cleavage of the C2-C3 bond of the LCB that eliminates an aldehyde ($C_{13}H_{27}CH{=}CHCHO$, 238 Da) residue and form an *N*- acylaminoethanol (NAE) anion ($C_{23}H_{45}CONHCH_2CH_2O^-$) at *m/z* 408 (a1). This bond cleavage is consistent with the observation of the deprotonated aldehyde anion of *m/z* 237 ($[C_{13}H_{27}CH{=}CHCHO - H]^-$) (b5) arising from loss of NAE leaving the charge on the LCB. The loss of H_2 from *m/z* 408 gave rise to a deprotonated *N*-nervonoylaminoethylen-1-ol ion at *m/z* 406 ($C_{23}H_{45}CONHCH{=}CHO^-$) (a2), which rearranged to a carboxyethenolamine anion ($C_{23}H_{45}COOCH{=}CHNH^-$) before forming a carboxylate anion at *m/z* 365 ($C_{23}H_{45}CO_2^-$) (a4) by loss of an azirine (41 Da) residue (Scheme 2a, route *a*). The observation of the carboxylate anion (RCO_2^-) ion of *m/z* 365 reflecting the 24:1-fatty acyl group provides the most useful information to identify the FA moiety of the molecule. Loss of H_2O from *m/z* 408 yielded ions of *m/z* 390 (a3), which further expelled an aziridine (43 Da) to *m/z* 347 (Scheme 2a). The ion of m/z 347 can also arise from *m/z* 365 by loss of H_2O. These fragmentation processes have been previously supported by CID MS^n studies on the authentic *N*-acylaminoethanol and its H-D exchanged homologs [16] and further confirmed by accurate mass measurements using high resolution mass spectrometry (data not shown).

The mechanism(s) leading to formation of the ions at *m/z* 616 (646 - HCHO) (c2), and 628 are shown in Scheme 2b, and 1c, respectively. Further dissociation of the ions of *m/z* 616 gave rise to ions of *m/z* 598 and 268 (b2), arising from losses of H_2O and of the fatty acyl moiety as a ketene (loss of $C_{22}H_{45}CH{=}C{=}O$), respectively. The cleavage of the C(2)-N(CO) bond also gave rise to *m/z* 364 (a7) (Scheme 2b). Further dissociation of the ions of *m/z* 628 yielded ions of *m/z* 263 and 364, simultaneously (Scheme 2c, route c_1), as well as the ion pair of *m/z* 237 and 390 (*route* c_2), indicating that the ions of *m/z* 628 may consist of an oxetane ring. These fragmentation pathways were supported by the MS^3 spectra of the ions of *m/z* 616 (646 → 616) and of 628 (646 → 628) (data not shown).

The ion of *m/z* 614 arose from loss of [H_2 + HCHO] residues (Scheme 3a) and gave rise to ions of *m/z* 420, 404, and 266 by further elimination of a $C_{12}H_{25}C{\equiv}CH$, $C_{13}H_{27}CH{=}CH_2$, and a $C_{22}H_{43}CH{=}C{=}O$ residue, respectively (646 → 614; Fig 1b). The spectrum (Figure 1b) also contained the acylamine anion of *m/z* 364 ($RCONH^-$), the ions of *m/z* 596 (614 - H_2O), and of *m/z* 404, representing a stable N-acyl, N-dehydroepoxide anion (a2). MS^3 on the ions of *m/z* 404 (646 → 614 → 404; Figure 1c) yielded ions at *m/z* 306 and 250 arising from charge-remote fragmentations with β-cleavage and γ-H shift (allylic bond cleavages) (Scheme 3a). The presence of these ions demonstrated that the double bond is located at C-15 of the 24:1-fatty acyl chain [31].

The MS^2 spectrum of the d18:1/18:1-Cer at *m/z* 562 (Table 1), and the MS^3 spectrum of the ions of *m/z* 530 (562 → 530) (not shown) contained analogous ions arising from the same fragmentation processes. MS^4 on the ions of *m/z* 320 (562 → 530 → 320; Figure 1d) gave rise to ions of *m/z* 242 and 186 arising from the similar CRF processes involving β-cleavage with γ-H shift, leading to locate the double bond at C-9 [31] (Scheme 3b).

3.2. Identification of N-acyl sphinganine (d18:0/nFA-Cer) (Cer[NdS] and N-α-hydroxyacyl sphinganine (d18:0/αhFA-Cer) (Cer[AdS])

One of the feature in the product–ion spectrum of the *N*-acylsphinganine is that the [M – H - HCHO]$^-$ ion is nearly absent, when acquired under an optimal collision energy. For example, the MS^2 spectrum of the d18:0/24:0Cer at *m/z* 650 (Figure 2a) contained abundant ions at *m/z* 632 (650 – H_2O), 618 (650 - [H_2 + HCHO]) and 602 (650 – H_2O - HCHO), but ions at *m/z* 620 (650 – HCHO) is not observed. The saturation in the LCB also alters the fragmentation processes. For example, the RCONH$^-$ ions (a7) at *m/z* 366 become less prominent, and ions at *m/z* 268 (618 – $C_{22}H_{45}CH{=}C{=}O$) arising from further loss of the fatty acyl ketene become visible; and the ion at *m/z* 269, analogous to *m/z* 267 seen for d18:1/nFA-Cer is absent. These differences indicate that cleavage of N-CO bond to eliminate a fatty acyl ketene is a more facile fragmentation process than cleavage the N(CO)-C2 bond that formed the RCONH$^-$ ions for N-acylsphinganine ceramide family. Other ions characteristic to this ceramide family were observed at *m/z* 300 (b1), representing an 18:0-sphinganine anion, and at *m/z* 239 (b5) representing an anionic aldehyde ion arising from cleavage of the C2-C3(OH) bond of the LCB (Scheme 4a). Cleavage of the same C2-C3(OH) bond with simultaneous release of H_2 also led to the ion of *m/z* 408 (*c*1), in which the charge may reside at the oxygen attached to C1 (Scheme 4a, route *c*). The ions of *m/z* 300 and 239 are 2 Da heavier than the ions of *m/z* 298 and 237 observed for N-acylsphingosine, consistent with the cleavages of bonds as proposed. The above fragmentation processes were further supported by the MS^2 spectrum of the d18:0/18:0-Cer at *m/z* 566 (Table 1), which contains the analogous ions. The differences in the ions formed by d18:0/nFA and d18:1/nFA, provide structural differentiation between these two ceramide families.

The substitution of nFA by αhFA in the structure facilitates the fragmentations, leading to substantial change in the MS^n spectra of d18:0/hFA-Cer. For example, the LCB anions at *m/z* 300 are prominent in the MS^2 spectrum of the d18:0/αh16:0-Cer at *m/z* 554 (Figure 2b), due to loss of the fatty acid moiety as [CO + $C_{14}H_{29}CHO$] (Scheme 4b). Similar cleavage of CO-C2(OH) bond also led to *m/z* 328 (b8) by loss of an aldehyde ($C_{14}H_{29}CHO$). The ions at *m/z* 271 (a6), 253 (a8) and 225 (a9) are indications of αh16:0-FA (described later). Other noticeable ions observed at *m/z* 314 (a1), 312 (a2), and 296 (a3), arose from the similar cleavages of the LCB. All the ions related to LCB such as ions at *m/z* 286 (b1) and 254 (b3) 225 (b5) are 14 Da (CH_2) lighter in the MS^2 spectrum of d17:0/αh16:0-Cer at *m/z* 540 (Table 1), consistent with the structure.

3.3. Characterization of t18:0/nFA-Cer (Cer[NP]) and t18:0/αhFA-Cer (Cer[AP])

The fragmentations of the molecules were facilitated by the hydroxyl group at C-4 of the phytosphingosine LCB and the α-hydroxyl group on the fatty acyl substituent, resulting in drastic decline in the common ions that distinct them from other ceramide families. Figure 3a illustrated the MS^2 spectrum of the t18:0/20:0-Cer at *m/z* 610, which contained the ions at *m/z* 592 (c1), 578 (c4), 574 (c5), and 580 (c2). The low abundance of the common ions observed in the spectrum is consistent with the presence of abundant NAE anions of *m/z* 354 and of RCO_2^- ion of *m/z* 311 ($C_{19}H_{39}CO_2^-$), arising from the fragmentation processes activated by the hydroxyl groups. The cleavage of the C2-C3(OH) bond with charge residing

on the fatty acyl end and LCB, respectively, gave rise to NAE anion of *m/z* 354 (a1), and α-hydroxyaldehyde anion of *m/z* 255 (b5) (Scheme 5a). The ions of *m/z* 354 undergo rearrangement and dissociate to ions of *m/z* 311 by loss of azetane. The pathway led to *m/z* 592 possessing an oxetane ring due to loss of H_2O is similar to that shown in Scheme 2c. Further dissociation of *m/z* 592 (610 → 592; Figure 3b) gave rise to ions of *m/z* 366 (592 – $C_{14}H_{29}CHO$) and aldehyde anions of *m/z* 225 ($C_{13}H_{27}CH{=}CHO^-$), simultaneously, via cleavage of the C3-C4(OH) bond (b_1 cleavage) activated by the 4-OH group; and ions of *m/z* 336 and 255 (b_2 cleavage) from cleavages across the oxetane ring; while cleavage of C(2)-N (CO) bond (b_3 cleavage) yielded ions of *m/z* 310 and 281, simultaneously (Scheme 5b). Further dissociation of ions of 578 (c4) also gave rise to the acylamine anion ($C_{19}H_{39}CONH^-$) at *m/z* 310 and ions of *m/z* 267 via cleavage of the C2-C3(OH) bond (Scheme 5c). The above fragmentation processes were supported by the MS^3 spectra of the ions of *m/z* 592 (610 → 592) and 578 (610 → 578) (data not shown). Ions of *m/z* 267 and 255 are diagnostic ions for recognition of the C-18 phytosphigosine (t18:0-LCB). Analogous ions at *m/z* 239 and 227 were observed in the MS^2 spectrum of t16:0/18:0-Cer at *m/z* 554 (Table 1).

Extensive fragmentations were also observed for t18:0/αhFA-Cer. Thus, the MS^2 spectrum of the $[M - H]^-$ ion of t18:0/αh20:0-Cer at *m/z* 626 (Figure 3c) contained prominent RCO_2^- ion at *m/z* 327 and the NAE anion at *m/z* 370 reflecting fatty acyl substituent, while ions of *m/z* 608 (c1), 596 (c2), 594 (c3), 590 (c4) and 578 (c5) are of low abundances. The ions recognizing the t18:0-LCB component were also observed at *m/z* 267 (b6) and 255 (b5). The ions of *m/z* 309 and 281 arose from further dissociation of the RCO_2^- ion of *m/z* 327 ($C_{18}H_{37}CH(OH)CO_2^-$) by elimination of an H_2O and $[H_2 + CO_2]$ residues, respectively. This fragmentation process was supported by MS^3 on the ions of *m/z* 327 (626 → 327, Figure 3d). The formation of the ions of *m/z* 327 (RCO_2^-), 309 (RCO_2^- - H_2O) and 281 (RCO_2^- - $[H_2 + CO_2]$) is characteristic to the αh20:0-fatty acid, providing its differentiation from other ceramides containing nonhydroxy-, β-hydroxy, or ω-hydroxy-fatty acid moiety. The observation of the ions of *m/z* 239 (b6) and 227 (b5), which are 28 Da (C_2H_2) lighter than the ions of *m/z* 267 and 255, respectively, in the MS^2 spectrum of t16:0/αh20:0-Cer at *m/z* 598 (Table 1) is consistent with the presence of t16:0-LCB.

3.4. Distinction of N-α-hydroxyacylsphing-4-enines (d18:1/αhFA-Cer) (Cer[AS]), N-β-hydroxyacylsphing-4-enines (d18:1/βhFA-Cer) (Cer[BS]) and N-ω-hydroxyacylsphing-4-enines (d18:1/ωhFA-Cer) (Cer[OS])

The $[M – H]^-$ ions at *m/z* 664 (d18:1/αh24:0-Cer), 692 (d18:1/βh26:0-Cer), and 776 (d18:1/ωh32:0-Cer) representing ceramides consisting of sphingosine-LCB with α-, β-, and ω-hydroxyl fatty acid substituents, respectively, were investigated. As shown in Figure 4a, common ions at *m/z* 646 ($[M - H - H_2O]^-$) (c1), 634 ([M - H - HCHO]- (c2), and 632 (([M - H – H_2 - HCHO]$^-$ (c3), 628 ($\underline{c}_1$ - $H_2O]^-$) (c4) and 616 (c1 – HCHO) (c5) in the MS^2 spectrum of the $[M - H]^-$ ions of d18:1/αh24:0-Cer at *m/z* 664, where ions at *m/z* 646, 628 and 616 involving water loss are more abundant than those seen in the d18:1/nFA-Cer (§*3.4*) earlier due to the presence of α-hydroxyl group. The cleavage of the C2-C3 bond of the LCB followed by loss of H_2 led to the NAE anions of *m/z* 424 (a1), which expel an azetene to form 2-hydroxy tetraeicosanoic anions (RCO_2^-) of *m/z* 383 (a6), following a

rearrangement process as seen earlier. The observation of ions at *m/z* 365 (a8) and 337 (a9) from sequential losses of H_2O and [H_2 + CO_2], respectively, from the ion of *m/z* 383 (Scheme 6a) indicates the presence of αh24:0-FA. Other ions specific to d18:1/αhFA family was seen at *m/z* 268 (b2), arising from 634 ([M - H -HCHO]$^-$) (c2), which eliminates CO and the fatty acid substituent as a terminal aldehyde ($C_{22}H_{45}CHO$) by the facile fragmentation process activated by the α-OH of the fatty acyl substituent (Scheme 6b).

The MS^2 spectrum of d18:1/ωh32:0-Cer at *m/z* 776 (Figure 4b) is similar to that of d18:1/24:1-Cer (Figure 1a), excepting that the [M – H - HCHO – H_2O]$^-$ ion at *m/z* 728 (c5) ion is the most prominent, probably attributable to the presence of the ω-hydroxyl group that permits additional H_2O loss. The spectra similarity suggests that the fragmentation processes of d18:1/nFA-Cer and d18:1/ωhFA-Cer are similar. The ions reflecting the ωh32:0-fatty acyl substituent of the molecule were seen at *m/z* 495 (RCO_2^-), and 494 ($RCONH^-$), and the ions at *m/z* 298 (b1), 268 (b2), 263 (b4), and 237 (b5) recognizing the d18:1-LCB are of low abundance, similar to those observed for d18:1/nFA-Cer. Further dissociation of the ion of *m/z* 495 (776 → 495; Figure 4c) gave ions of *m/z* 477 (loss of H_2O) and 451 (loss of CO_2) and the spectrum is identical to the MS^2 spectrum of the [M – H]$^-$ ion of ω-OH 32:0-FA standard (data not shown), supporting the presence of ωh32:0-FA moiety.

In contrast, the MS^2 spectrum of d18:1/βh26:0-Cer at *m/z* 692 (Figure 4d) is dominated by the ion of *m/z* 340, arising from preferential cleavage of C2-C3(OH) bond of the fatty acyl group to release an aldehyde and resulted in a d18:1/2:0-Cer anion (scheme 7a). This facile bond cleavage led to the decline of the ions of *m/z* 674 (c1), 662 (c2), 660 (c3), and 664 (c5). The ions of *m/z* 674 (692 - H_2O) may represent a d18:1/26:1-Cer resulting from the H_2O loss involving the 2-OH group to become a 26:1-fatty acid (Scheme 7b). The MS^3 spectrum of the ions of *m/z* 340 (692→340; Figure 4e) is identical to the MS^2 spectrum of the authentic d18:1/2:0-Cer (data not shown); and the MS^3 spectrum of the ions of *m/z* 674 (692→674; Figure 4f) also contains ions characteristic to a d18:1/26:1-Cer, confirming the fragmentation processes.

3.5. Complete structural characterization of N-ω-hydroxyacyl-6-hydroxysphing-4-enine (t18:1/ωhFA-Cer) (Cer[OH]) and N-α-hydroxy-6-hydroxysphing-4-enine (t18:1/αhFA-Cer) (Cer[AH])

The t18:1/ωhFA-Cer family was found in human stratum corneum, where t18:1/ωh30:0-Cer is the most abundant [27, 30]. The MS^2 spectrum of the [M - H]$^-$ ions of t18:1/ωh30:0-Cer at *m/z* 764 (Figure 5a) is dominated by common ions at *m/z* 746 (764 – H_2O), 734 (764 – HCHO), and 716 (764 – HCHO - H_2O); and the ions at *m/z* 732 (loss of [HCHO + H_2]) (c3) was nearly absent. The ions of *m/z* 467 (RCO_2^-) and 466 ($RCONH^-$) reflecting the ω-hydroxytriacontanoic acid moiety (ωh30:0), and the ions at *m/z* 314 (b1) and 279 (b4) that identify the 6-hydroxysphingo-4-enine LCB are of low abundance. The prominence of the common (c) ions together with the decline of acyl-related (a) and of LCB-related (b) ions indicates that the molecule is more stable due to the extra-long fatty acyl chain. The indication of the presence of an additional 6-hydroxy group on the LCB [27, 30] was seen by the presence of the ions at *m/z* 314 (b1), 284 (b2) and 279 (b4), which are 16 Da (one oxygen) heavier than the analogous ions of m/z 298, 268 and 263 observed for the d18:1-

LCB ceramide. The MS^3 spectrum of the ion of *m/z* 314 (764 → 314; Figure 5b) contained ions at *m/z* 284, 266, 255, 223, and 197, arising from cleavages of the C-C(OH) bonds (Scheme 8a); and the MS^3 spectrum of the ion of *m/z* 279 (764 → 279; Figure 5c) also contained abundant ions of *m/z* 197 and 110/111, along with *m/z* 223 arising from similar cleavages of the C-C(OH) bonds. The observation of these ions points to the position of the OH group at C6 (Scheme 8a).

The cleavage of the C5-C6(OH) bond of the LCB gave rise to the ions of *m/z* 566 which yielded ions of *m/z* 548 and 530 via consecutive loss of H_2O; while cleavage of the C2-C3(OH) bond gave rise to ions of *m/z* 510, which further eliminated H_2O to form ions of *m/z* 492 (Scheme 8b). The observation of these ions due to the presence of the 6-OH group on the LCB distinguishes t18:1/ωhFA-Cer from other ceramide families.

In contrast, the $[M - H]^-$ ion of t18:1/αh24:0-Cer at *m/z* 680 (Figure 5d) undergoes more vigorous fragmentation when subjected to CAD with optimal energy, attributable to the presence of the α-hydroxyl group of the fatty acyl substituent. Product ions reflecting the 6-hydroxysphing-4-enine LCB were also seen at *m/z* 314 (b1), 284 (b2) and 279 (b4) and 253 (b5). The MS^3 spectra of the ions of *m/z* 314 and 279 (data not shown) are identical to those shown in Figure 5b and 5c, respectively. These results, again, readily locate the 6-OH group of the LCB. The ions at *m/z* 426 (a1), 424 (a2), 408 (a3), 383 (RCO_2^-) (a6), and 382 ($RCONH^-$) (a7) reflecting the h24:0 fatty acyl substituent are prominent. The ions of *m/z* 383 along with ions of *m/z* 365 (383 – H_2O), and 337 (383 – [H_2 + CO_2]) arising from further dissociation, indicates the presence of αh24:0-Fatty acyl substituent. The observation of the minor ions at *m/z* 482, 464, and 436 arising from the similar fragmentation processes as shown in Scheme 8b, is consistent with the presence of t18:1-LCB.

3.6. Characterization of ceramide in biological specimen with isobaric isomers

The application of the present method to reveal the complex ceramide structures in the biological sample is exemplified by characterization of the $[M – H]^-$ ion of *m/z* 710 isolated from human stratum corneum. The MS^2 spectrum (Figure 6a) contained low abundance common ions at *m/z* 692 (710 - H_2O), 678 (710 – [H_2 + HCHO]), 674 (692 – H_2O), along with prominent ion set of the 383 (RCO_2^-), 365 (RCO_2^- - H_2O), and 339 (RCO_2^- - H_2O - CO), pointing to the presence of αh24:0-fatty acid substituent. These ions were formed together with ions of *m/z* 344 ($[LCB – H]^-$) (b1), 295 (b6), 283 (b5) that are 28 Da (C_2H_4) heavier than ions of *m/z* 316 (b1), 267 (b6), and 255 (b5) seen for t18:0-LCB as shown in Figure 3a, signifying the presence of t20:0-LCB. The above results led to assign the t20:0/h24:0-Cer structure. The assignment is further supported by the presence of the ions of *m/z* 382 ($RCONH^-$) (a7), 426 ($[NAE –H]^-$) (a1), 438 ($RCONH^-$ + C_3H_4 (a10), and 408 ($RCON^-CH=CH_2$) (a3) reflecting h24:0-FA, and by the presence of 309 (b4) arising from t20:0-LCB.

A second set of ions at *m/z* 411 (RCO_2^-), 393 (RCO_2^- - H_2O), and 365 (RCO_2^- - H_2O - CO) reflecting the h26:0-fatty acid substituent, and the set of ions of *m/z* 316 (b1) ($[LCB – H]^-$), 267 (b6), and 255 (b5), signifying the presence of t18:0-LCB are also present in the spectrum, pointing to the presence of t18:0/h26:0-Cer. This assignment is consistent with the

presence of the ions of *m/z* 410 ($RCONH^-$) (a7), 454 ($[NAE –H]^-$) (a1), 466 ($RCONH^- + C_3H_4$) (a10), and 436 ($RCON^-CH=CH_2$) (a3) that reassured the presence of h26:0-FA.

Two other minor isomers of t22:0/h22:0- and t16:0/28:0-Cer are also present. The assignment of t22:0/h22:0-Cer is supported by observation of the ions at *m/z* 355 (a6), 337 (a8) (overlap with $C_{23}H_{47}CO_2^-$ - 46) and 309 (a9), along with *m/z* 354 ($RCONH^-$) (a7), 398 ($[NAE – H]^-$) (a1), 410 ($RCONH^- + C_3H_4O$) (a10), and 380 ($RCON^-CH=CH_2$) (a3) reflecting the presence of h22:0-fatty acid substituent, and the ion set of *m/z* 372 ($[LCB – H]^-$) (b1), 323 (b6), 311 (b5), signifying the presence of t22:0-LCB. The presence of t16:0/h28:0-Cer minor isomer is seen by the ions of z 439 (RCO_2^-), 421 (RCO_2^- - H_2O), and 393 (RCO_2^- - H_2O - CO) reflecting the h28:0-fatty acid substituent, along with the ion of *m/z* 239 (b6) (the ions expected at *m/z* 288 and 227 are too low to be seen) that identifies the t16:0-LCB.

The structural assignment were further supported by the MS^3 spectrum of the ion of *m/z* 678 (710 → 678; Figure 6b), which gave rise to major $RCONH^-$ ions (a7) at *m/z* 382, 410, 354, and 438 (abundances in the descending order), reflecting the h24:0-, h26:0-, h22:0- and h28:0-FA substituents, respectively, along with the b6 ions at *m/z* 295, 267, 323, and 239 reflecting the t20:0-, t18:0-, t22:0- and t16:0-LCB, respectively. The *m/z* 382/295, 410/267, 354/323, and 438/239 ion pairs gave assignment of t20:0/h24:0-Cer, t18:0/h26:0-Cer, t22:0/h22:0, and t16:0/h28:0-Cer structures, consistent with the identified structures.

4. Conclusions

The present study is the first time that LIT MS^n mass spectrometric approach towards complete structural characterization of ceramides as the $[M – H]^-$ ions is demonstrated. The various ceramide families included in this study all yield distinct MS^n spectra, thereby, differentiation of isobaric ceramide isomers can be achieved. The observation of multiple sets of fragment ions reflecting the fatty acid and the LCB substituents is essential, in particular, in the structural identification of ceramides in biological specimen that often consists of many isomers. In contrast, structural information obtained by LIT MS^n on the $[M + H]^+$ ions of ceramides is inadequate to give assignment of the location of the functional groups, such as the hydroxyl group and double bond of the molecules [21, 23, 32]. Complete characterization of the complex ceramide structures in human stratum corneum and in mouse epidermis using the present method is currently in progress in our laboratory.

Acknowledgments

The author acknowledges the support of US Public Health Service Grants P41-GM103422, P60-DK-20579, P30-DK56341, and 4R33HL120760-03.

References

1. Hannun YA, Luberto C. Ceramide in the eukaryotic stress response. Trends in Cell Biology. 2000; 10:73–80. [PubMed: 10652518]
2. Kolesnick RN, Krönke M. Regulation of ceramide production and apoptosis. Annual Review of Physiology. 1998; 60:643–665.

3. Okazaki T, Kondo T, Kitano T, Tashima M. Diversity and Complexity of Ceramide Signalling in Apoptosis. Cellular Signalling. 1998; 10:685–692. [PubMed: 9884019]
4. Obeid LM, Hannun YA. Ceramide: A stress signal and mediator of growth suppression and apoptosis. J. Cell. Biochem. 1995; 58:191–198. [PubMed: 7673327]
5. Chao MV. Ceramide: A Potential Second Messenger in the Nervous System. Molecular and Cellular Neuroscience. 1995; 6:91–96. [PubMed: 7551569]
6. Venable ME, Lee JY, Smyth MJ, Bielawska A, Obeid LM. Role of Ceramide in Cellular Senescence. J. Biol. Chem. 1995; 270:30701–30708. [PubMed: 8530509]
7. Garidel P, Fölting B, Schaller I, Kerth A. The microstructure of the stratum corneum lipid barrier: Mid-infrared spectroscopic studies of hydrated ceramide:palmitic acid:cholesterol model systems. Biophysical Chemistry. 2010; 150:144–156. [PubMed: 20457485]
8. Mizutani Y, Mitsutake S, Tsuji K, Kihara A, Igarashi Y. Ceramide biosynthesis in keratinocyte and its role in skin function. Biochimie. 2009; 91:784–790. [PubMed: 19364519]
9. Imokawa G, Akasaki S, Hattori M, Yoshizuka N. Selective recovery of deranged water-holding properties by stratum corneum lipids. J Invest Dermatol. 1986; 87:758–761. [PubMed: 3782858]
10. Imokawa G, Akasaki S, Minematsu Y, Kawai M. Importance of intercellular lipids in water-retention properties of the stratum corneum: induction and recovery study of surfactant dry skin. Arch Dermatol Res. 1989; 281:45–51. [PubMed: 2730142]
11. Polito AJ, Akita T, Sweeley CC. Gas chromatography and mass spectrometry of sphingolipid bases. Characterization of sphinga-4,14-dienine from plasma sphingomyelin. Biochemistry. 1968; 7:2609–2614. [PubMed: 5660077]
12. Raith K, Darius J, Neubert RHH. Ceramide analysis utilizing gas chromatography–mass spectrometry. Journal of Chromatography A. 2000; 876:229–233. [PubMed: 10823518]
13. Ann Q, Adams J. Structure determination of ceramides and neutral glycosphingolipids by collisional activation of [M + Li]+ ions. J. Am. Soc. Mass Spectrom. 1992; 3:260–263. [PubMed: 24242949]
14. Ann Q, Adams J. Structure-specific collision-induced fragmentations of ceramides cationized with alkali-metal ions. Anal. Chem. 1993; 65:7–13.
15. Gu M, Kerwin JL, Watts JD, Aebersold R. Ceramide Profiling of Complex Lipid Mixtures by Electrospray Ionization Mass Spectrometry. Anal. Biochem. 1997; 244:347–356. [PubMed: 9025952]
16. Hsu F-F, Turk J. Characterization of ceramides by low energy collisional-activated dissociation tandem mass spectrometry with negative-ion electrospray ionization. J. Am. Soc. Mass Spectrom. 2002; 13:558–570. [PubMed: 12019979]
17. Hsu F-F, Turk J, Stewart ME, Downing DT. Structural studies on ceramides as lithiated adducts by low energy collisional-activated dissociation tandem mass spectrometry with electrospray ionization. J Am Soc Mass Spectrom. 2002; 13:680–695. [PubMed: 12056568]
18. Sullards MC, Merrill AH Jr. Analysis of sphingosine 1-phosphate, ceramides, and other bioactive sphingolipids by high-performance liquid chromatography-tandem mass spectrometry. Sci STKE. 2001; 30
19. Han X. Characterization and direct quantitation of ceramide molecular species from lipid extracts of biological samples by electrospray ionization tandem mass spectrometry. Anal Biochem. 2002; 302:199–212. [PubMed: 11878798]
20. Masukawa Y, Narita H, Shimizu E, Kondo N, Sugai Y, Oba T, Homma R, Ishikawa J, Takagi Y, Kitahara T, Takema Y, Kita K. Characterization of overall ceramide species in human stratum corneum. J. Lipid Res. 2008; 49:1466–1476. [PubMed: 18359959]
21. t'Kindt R, Jorge L, Dumont E, Couturon P, David F, Sandra P, Sandra K. Profiling and characterizing skin ceramides using reversed-phase liquid chromatography- quadrupole time-of-flight mass spectrometry. Anal Chem. 2012; 84:403–411. [PubMed: 22111752]
22. Liebisch G, Drobnik W, Reil M, Trümbach B, Arnecke R, Olgemöller B, Roscher A, Schmitz G. Quantitative measurement of different ceramide species from crude cellular extracts by electrospray ionization tandem mass spectrometry (ESI-MS/MS). J. Lipid Res. 1999; 40:1539–1546. [PubMed: 10428992]

23. van Smeden J, Hoppel L, van der Heijden R, Hankemeier T, Vreeken RJ, Bouwstra JA. LC/MS analysis of stratum corneum lipids: ceramide profiling and discovery. J. Lipid Res. 2011; 52:1211–1221. [PubMed: 21444759]

24. Raith K, Neubert RHH. Structural studies on ceramides by electrospray tandem mass spectrometry. Rapid Commun. Mass Spectrom. 1998; 12:935–938.

25. Vietzke JP, Brandt O, Abeck D, Rapp C, Strassner M, Schreiner V, Hintze U. Comparative Investigation of Human Stratum Corneum Ceramides. Lipids. 2001; 36:299–304. [PubMed: 11337986]

26. Stewart ME, Downing DT. Free Sphingosines of Human Skin Include 6- Hydroxysphingosine and Unusually Long-Chain Dihydrosphingosines. Journal of Investigative Dermatology. 1995; 105:613–618. [PubMed: 7561168]

27. Stewart ME, Downing DT. A new 6-hydroxy-4-sphingenine-containing ceramide in human skin. J. Lipid Res. 1999; 40:1434–1439. [PubMed: 10428979]

28. Wertz PW, Madison KC, Downing DT. Covalently bound lipids of human stratum corneum. J Invest Dermatol. 1989; 92:109–111. [PubMed: 2909622]

29. Motta S, Monti M, Sesana S, Caputo R, Carelli S, Ghidoni R. Ceramide composition of the psoriatic scale. Biochimica et Biophysica Acta (BBA) - Molecular Basis of Disease. 1993; 1182:147–151. [PubMed: 8357845]

30. Robson KJ, Stewart ME, Michelsen S, Lazo ND, Downing DT. 6-Hydroxy-4-sphingenine in human epidermal ceramides. J. Lipid Res. 1994; 35:2060–2068. [PubMed: 7868984]

31. Hsu F-F, Turk J. Distinction among isomeric unsaturated fatty acids as lithiated adducts by electrospray ionization mass spectrometry using low energy collisionally activated dissociation on a triple stage quadrupole instrument. J. Am. Soc. Mass Spectrom. 1999; 10:600–612. [PubMed: 10384724]

32. Farwanah H, Pierstorff B, Schmelzer CEH, Raith K, Neubert RHH, Kolter T, Sandhoff K. Separation and mass spectrometric characterization of covalently bound skin ceramides using LC/APCI-MS and Nano-ESI-MS/MS. J. Chromatogr. B. 2007; 852:562–570.

Highlights

- Complete structural characterization of ceramides in 10 subfamilies is presented
- Linear ion-trap multiple stage mass spectrometry provides structural details and reveals the mechanisms underlying the fragmentation processes
- Multiple sets of fragment ions regarding to fatty acid and long chain base substituents lead to confident structure assignment and isomer differentiation
- Isomeric structures in a biological specimen are identified

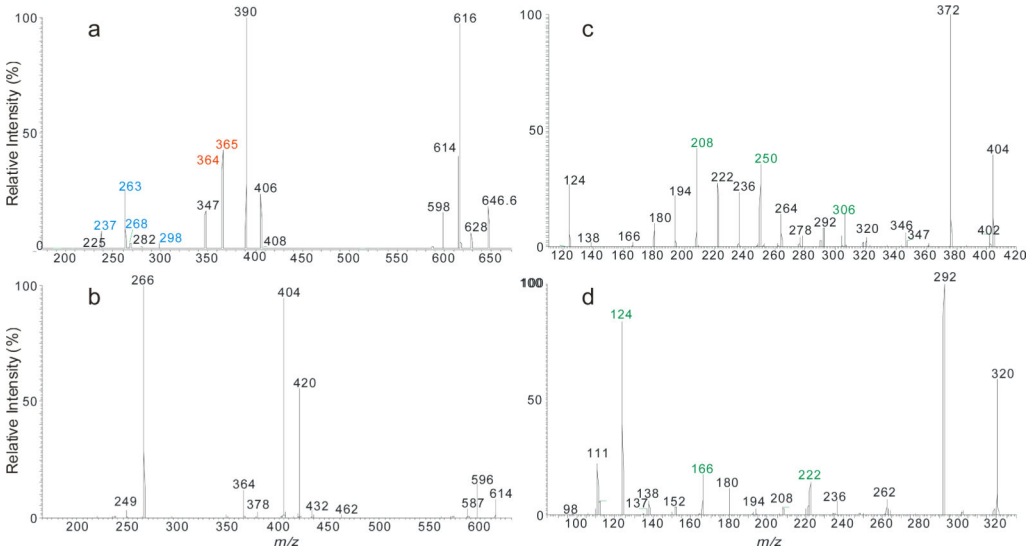

Figure 1.

The LIT MS^2 spectrum of the $[M - H]^-$ ions of d18:1/24:1-Cer at *m/z* 646 (a), its MS^3 spectrum of the ions of *m/z* 614 (646 → 614) (b), MS^4 spectrum of the ions of *m/z* 404 (646 → 614 → 404) (c), and the MS^4 spectrum of the ions of *m/z* 320 (562 → 530 → 320) (d), arising from d18:1/18:1-Cer. The MS^4 spectra locate the double bond of the fatty acyl chain.

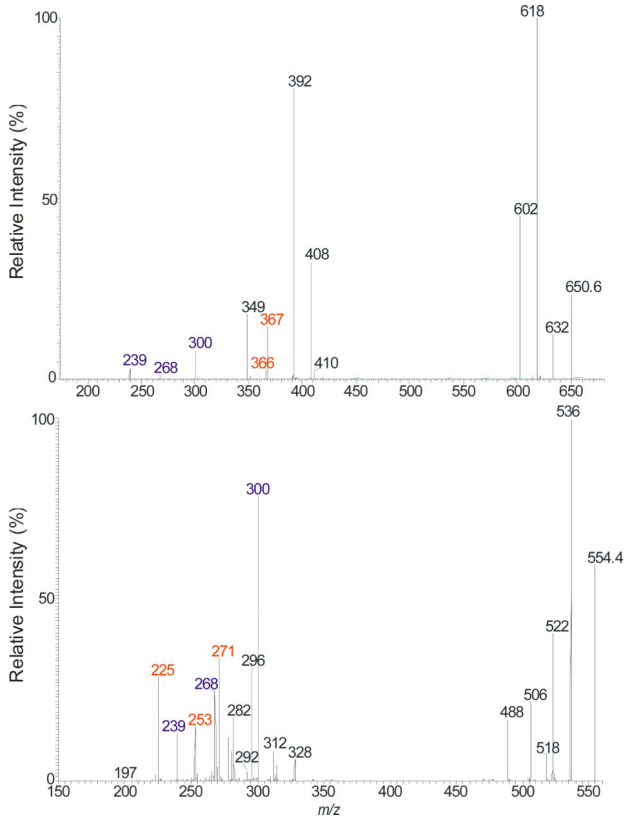

Figure 2.

The LIT MS^2 spectrum of the $[M - H]^-$ ions of d18:0/24:0-Cer at *m/z* 650 (a), and of d18:1/αh16:0-Cer at *m/z* 554 (b).

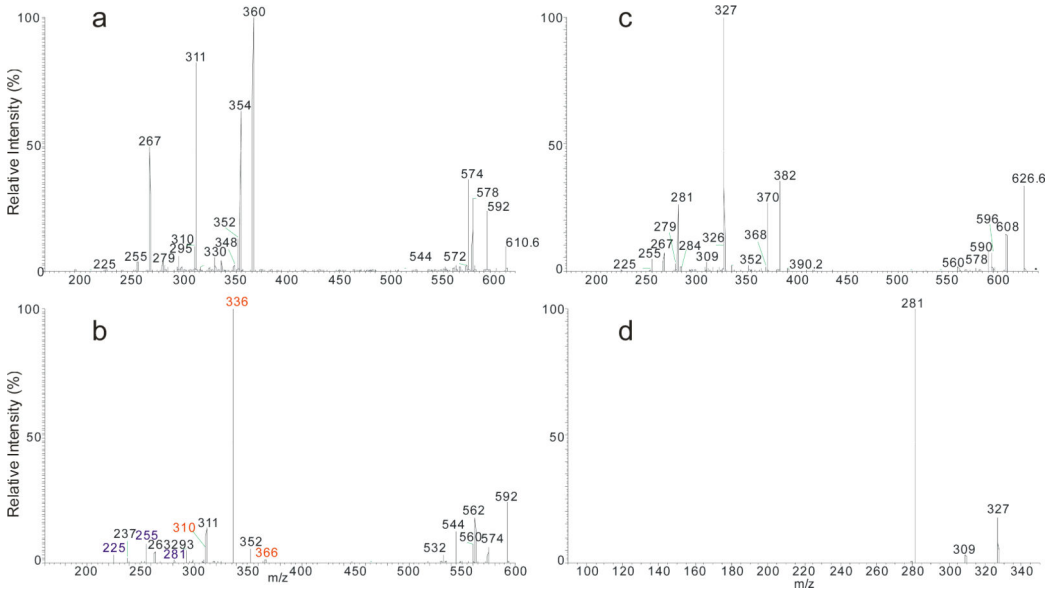

Figure 3.

The MS^2 spectrum of the $[M - H]^-$ ions of t18:0/20:0-Cer at *m/z* 610 (a), its MS^3 spectrum of the ions of *m/z* 592 (610 → 592) (b); and the MS^2 spectrum of the $[M - H]^-$ ions of t18:0/h20:0-Cer at *m/z* 626 (c), its MS^3 spectrum of the ions at *m/z* 327 (626 → 327) (d).

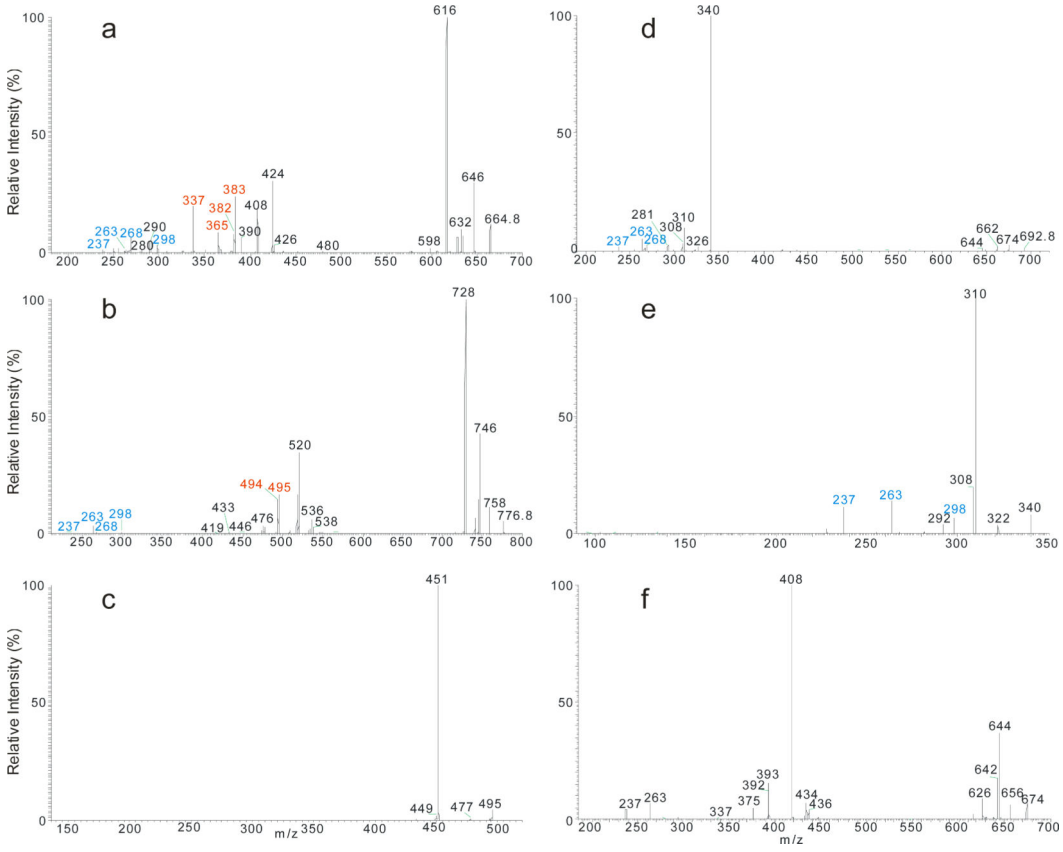

Figure 4.

The MS^2 spectrum of the $[M - H]^-$ ions of d18:1/h24:0-Cer at *m/z* 664 (a), of d18:1/ω32:0-Cer at *m/z* 776 (b), and it MS^3 spectrum of the ions of *m/z* 495 (776 → 495) (c); and the MS^2 spectrum of the $[M - H]^-$ ions of d18:1/βh26:0-cer at *m/z* 692 (d), its MS^3 spectra of the ion of *m/z* 340 (692 → 340) (e), and of *m/z* 674 (692 → 674) (f). The MS^3 spectra of *m/z* 340, and *m/z* 674, are identical to the MS^2 spectra of the $[M - H]^-$ ions of d18:1/2:0-Cer, and d18:1/26:1-Cer respectively, leading to define the d18:1/βh26:0-Cer structure (see Scheme 7 for detail).

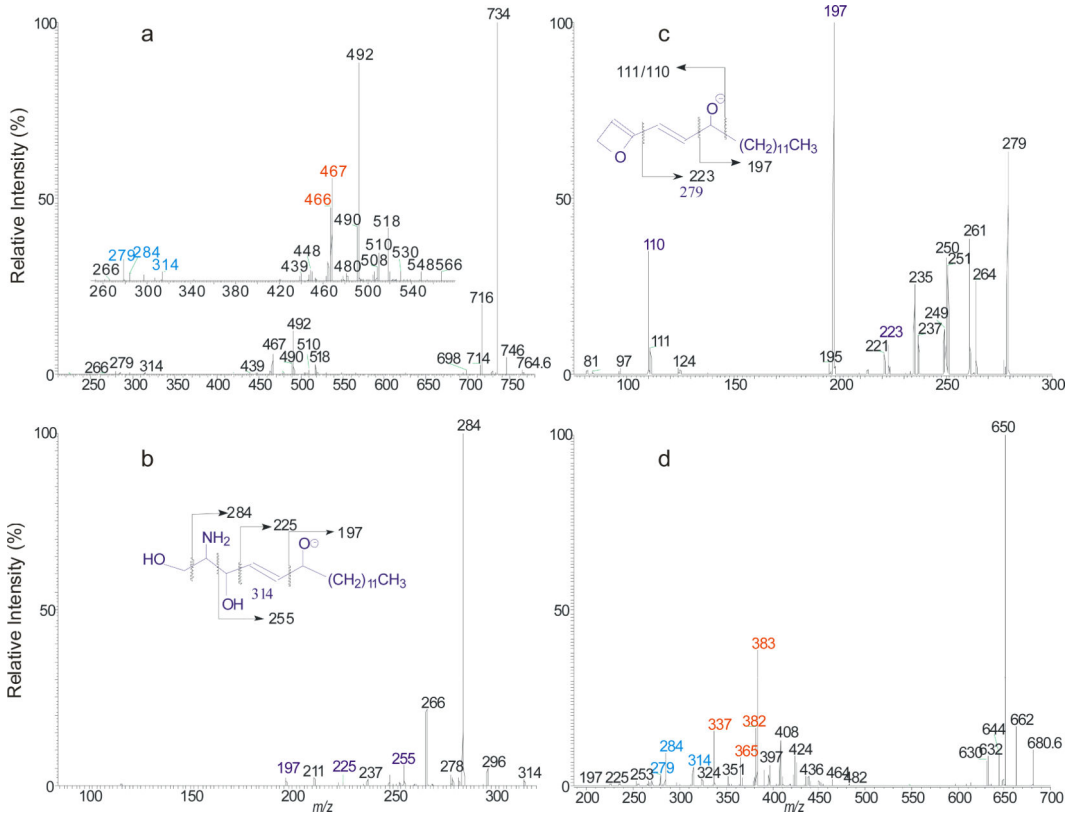

Figure 5.

The MS^2 spectrum of the $[M - H]^-$ ions of t18:1/ω30:0-Cer at m/z 764 (a), its MS^3 spectra of the ions of *m/z* 314 (764→ 314) (b), and of *m/z* 279 (764→ 279) (c), and the MS^2 spectrum of the $[M - H]^-$ ions of t18:1/αh24:0-Cer at *m/z* 680 (d).

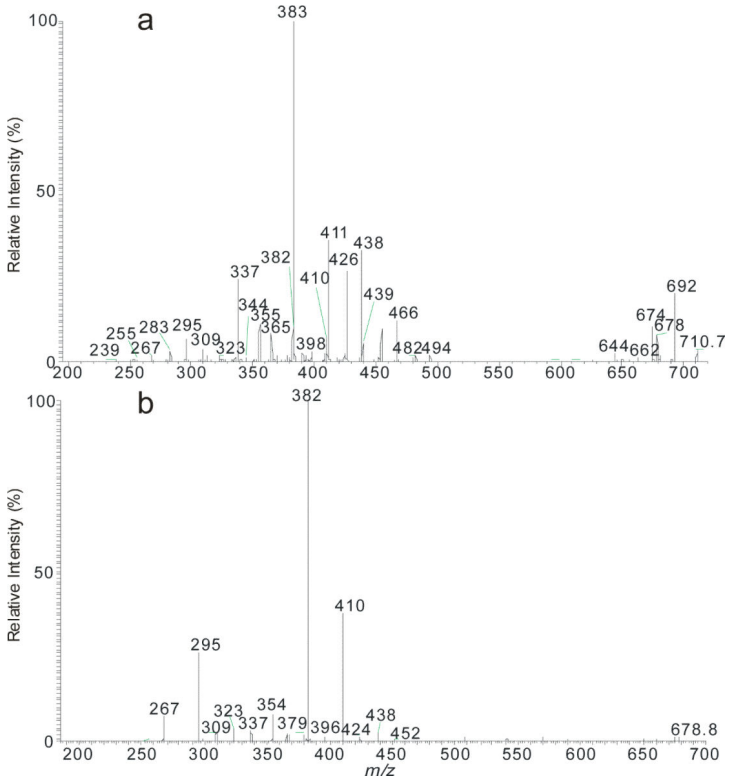

Figure 6.

The MS^2 spectrum of the $[M - H]^-$ ions of a phytosphingosine-LCB with αhFA ceramide at *m/z* 710 isolated from stratum corneum (a), and its MS^3 spectra of the ions of *m/z* 678 (710→ 678) (b). The spectra contained multiple sets of ions leading to define the multiple isomeric structures.

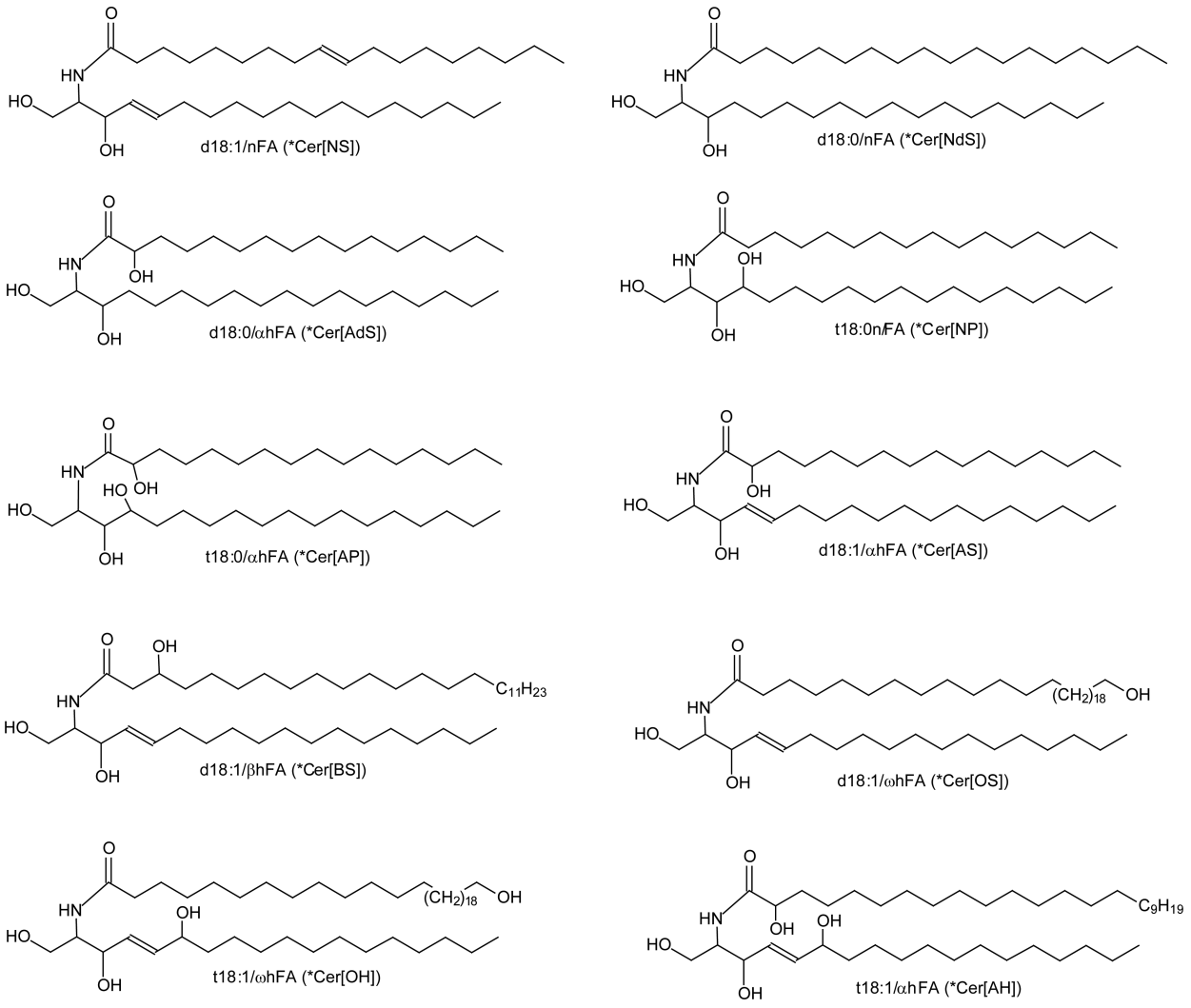

Scheme 1.

Structures of 10 ceramide subfamilies included in this study. Designation in (*Parenthesis) is nomenclature of Motta et al.[29], expanded by Robson et al [30] and Masukawa et al [30]. In this system, the initial letter of the sphingoid base: S, dS, P, and H represent sphingosine, dihydrosphingosine, phytosphingosine, and 6-hydroxysphingosine, respectively; the fatty acid residues: N, A, O, and B represent nonhydroxylated acyl, a-hydroxyacyl, b-hydroxyacyl, and w-hydroxyacyl, respectively. As shown are ceramides with C18-LCB. More cermide structures please see Table 1.

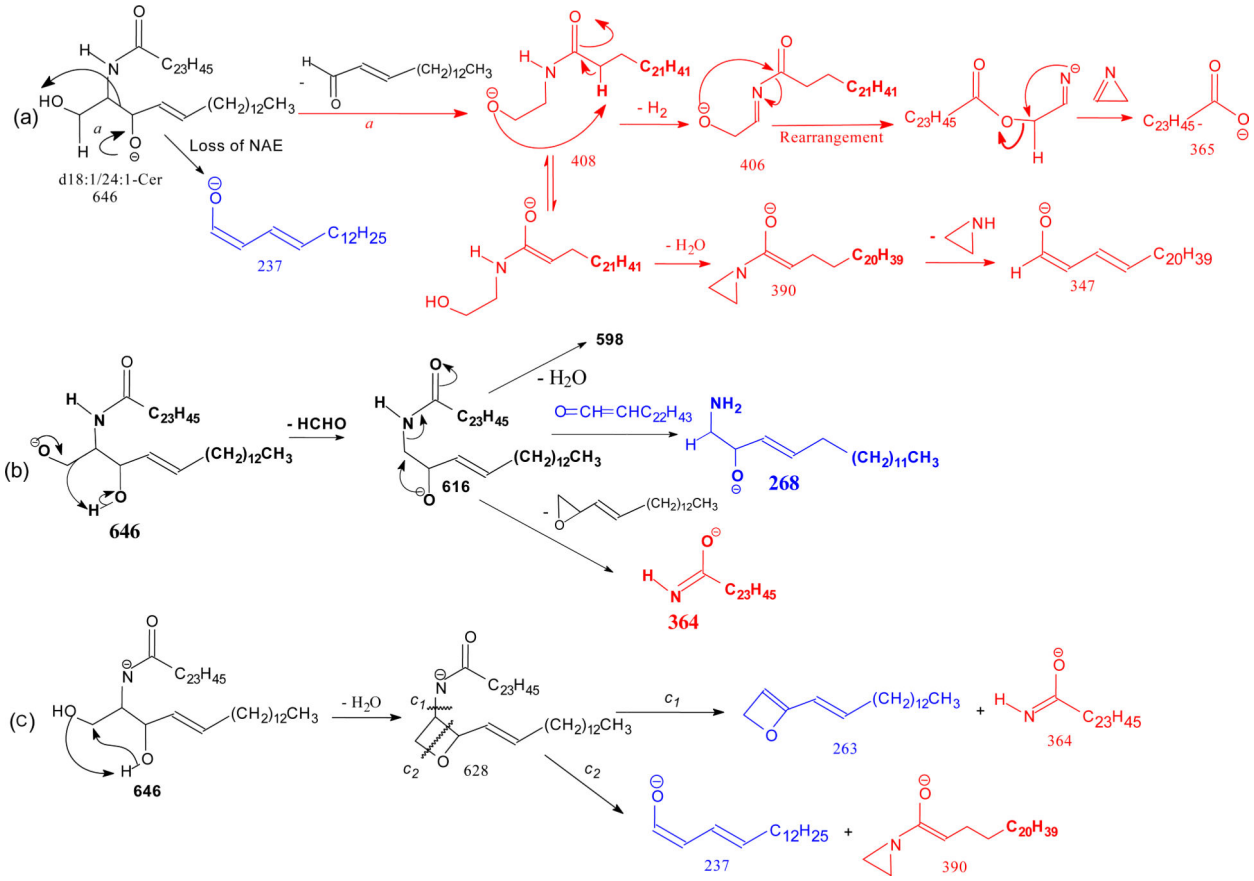

Scheme 2.

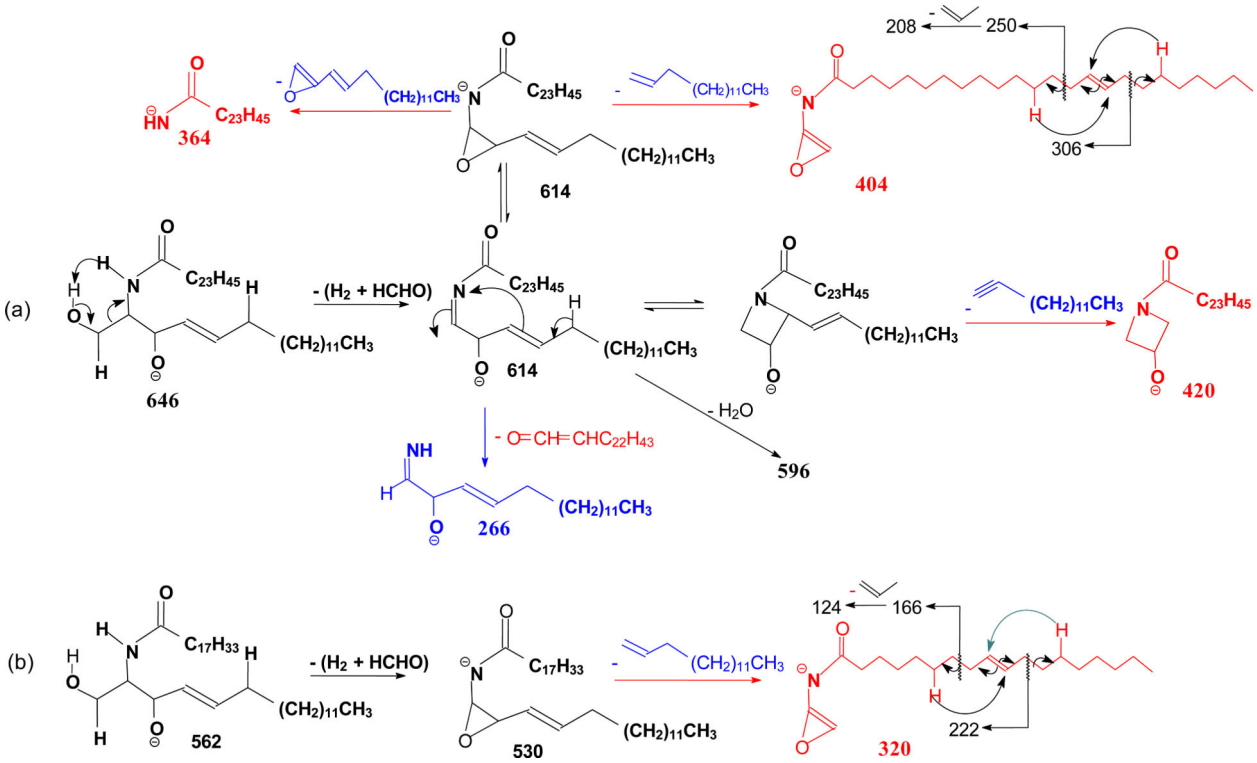

Scheme 3.

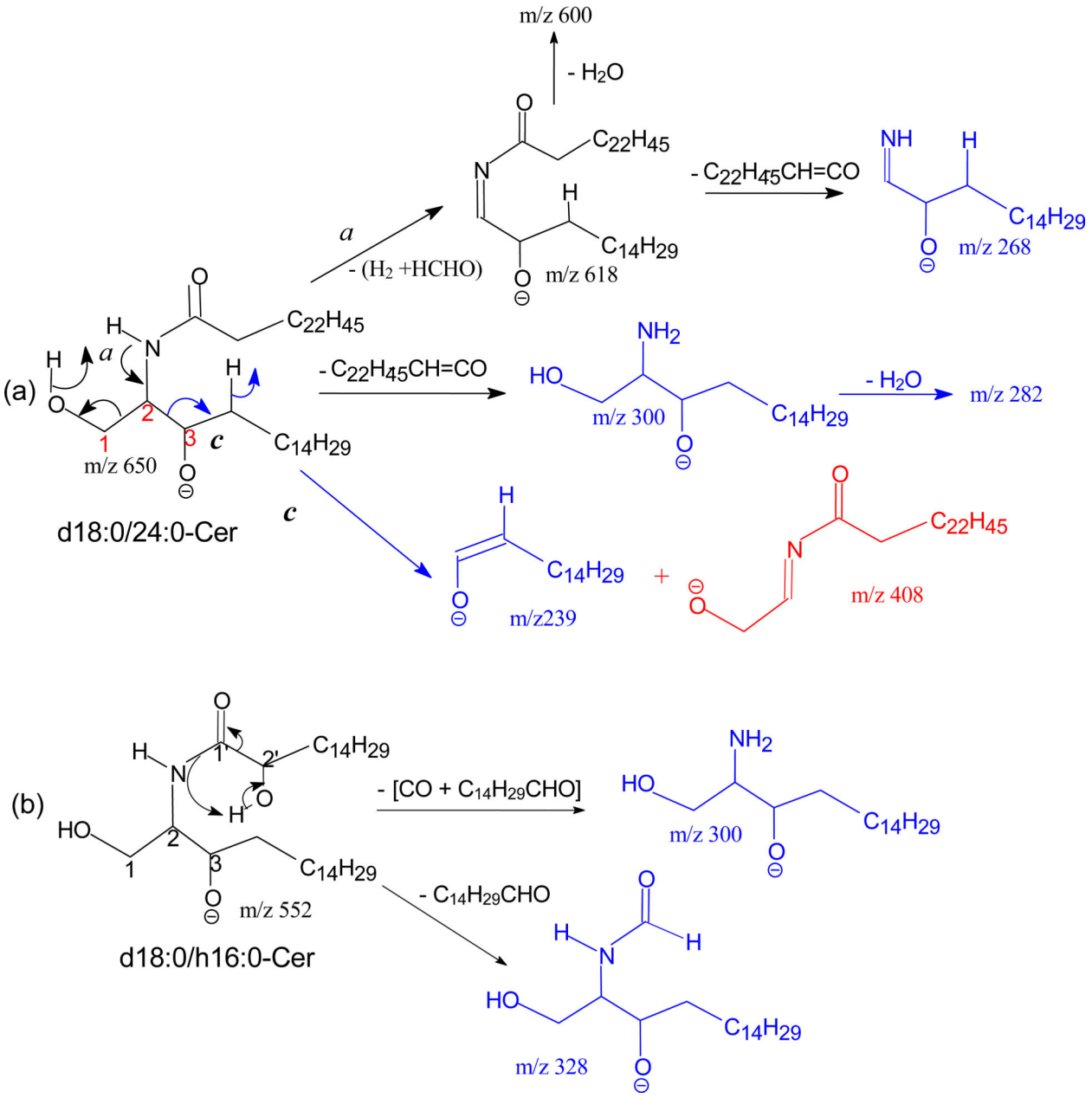

Scheme 4.

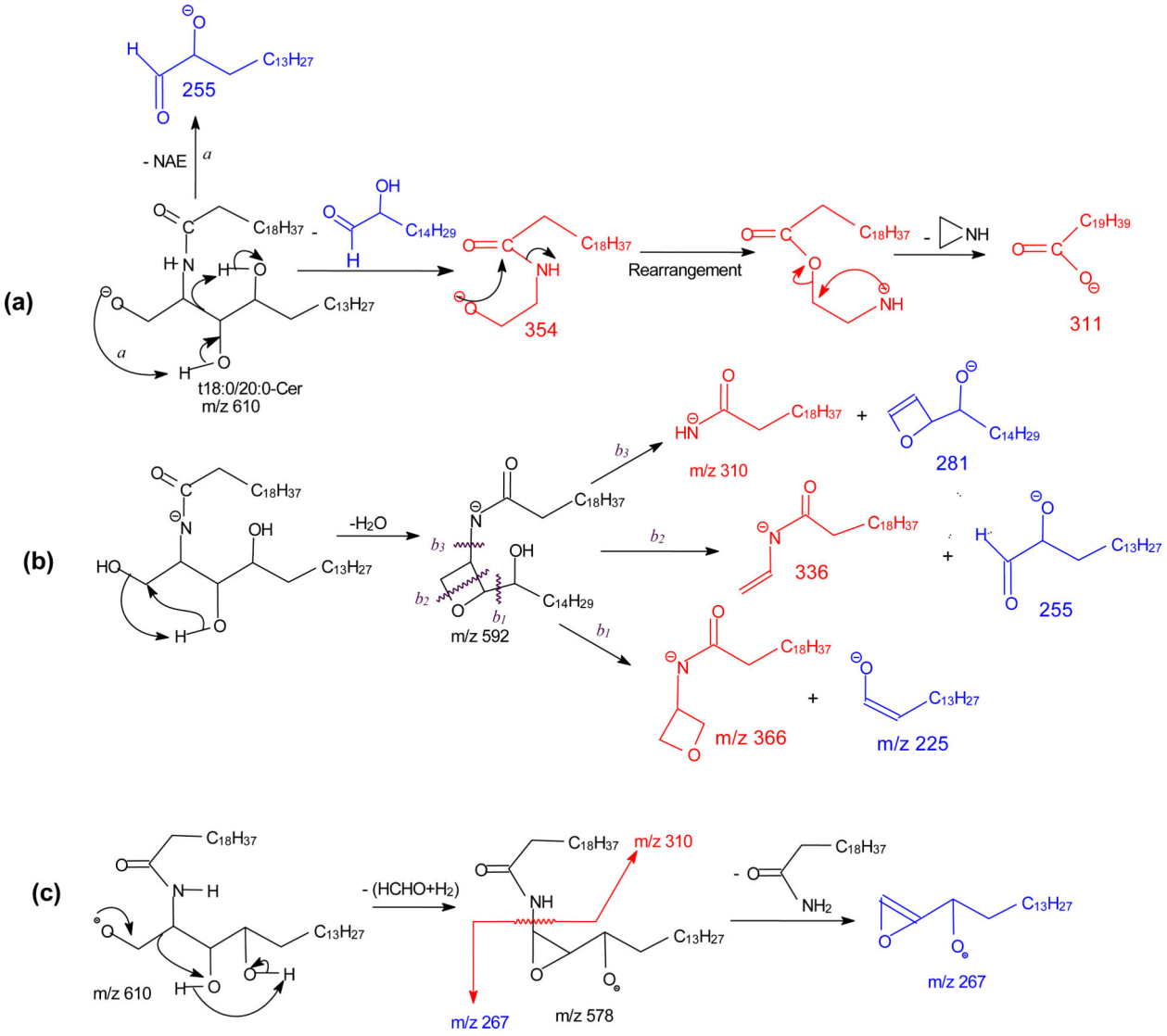

Scheme 5.

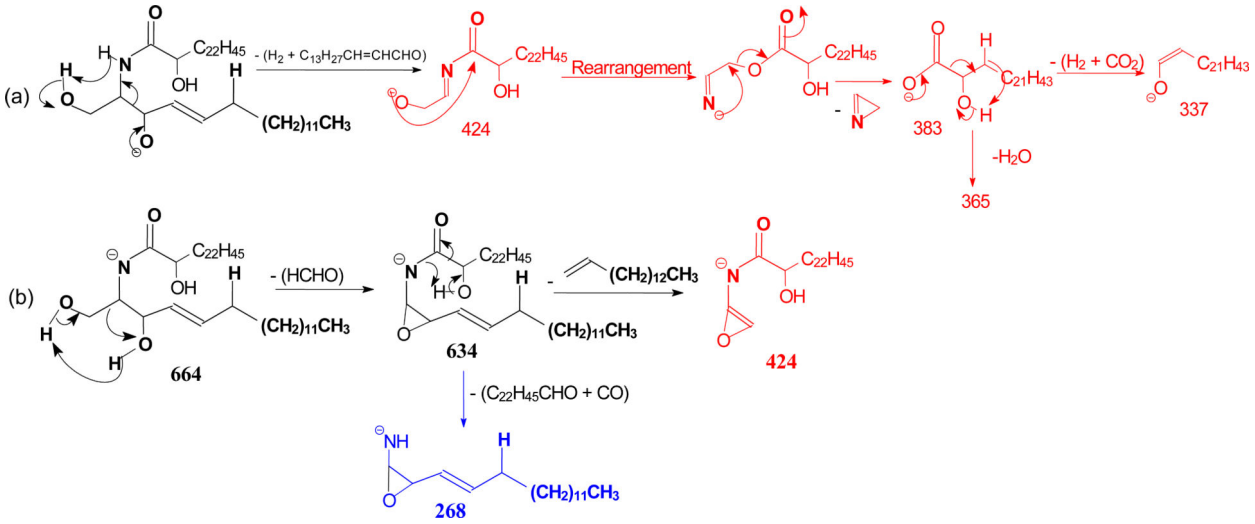

Scheme 6.

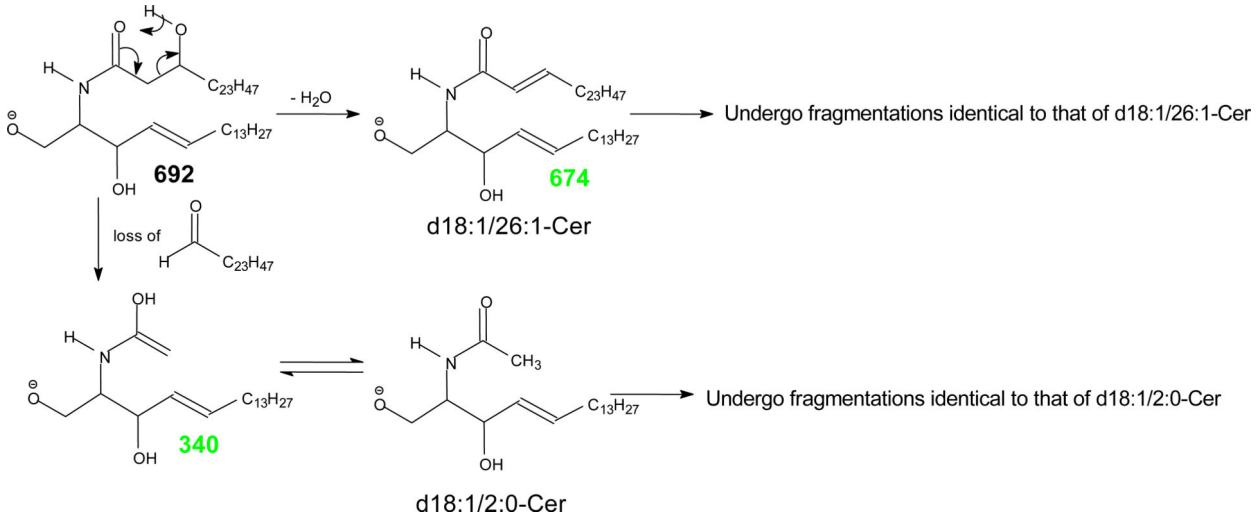

Scheme 7.

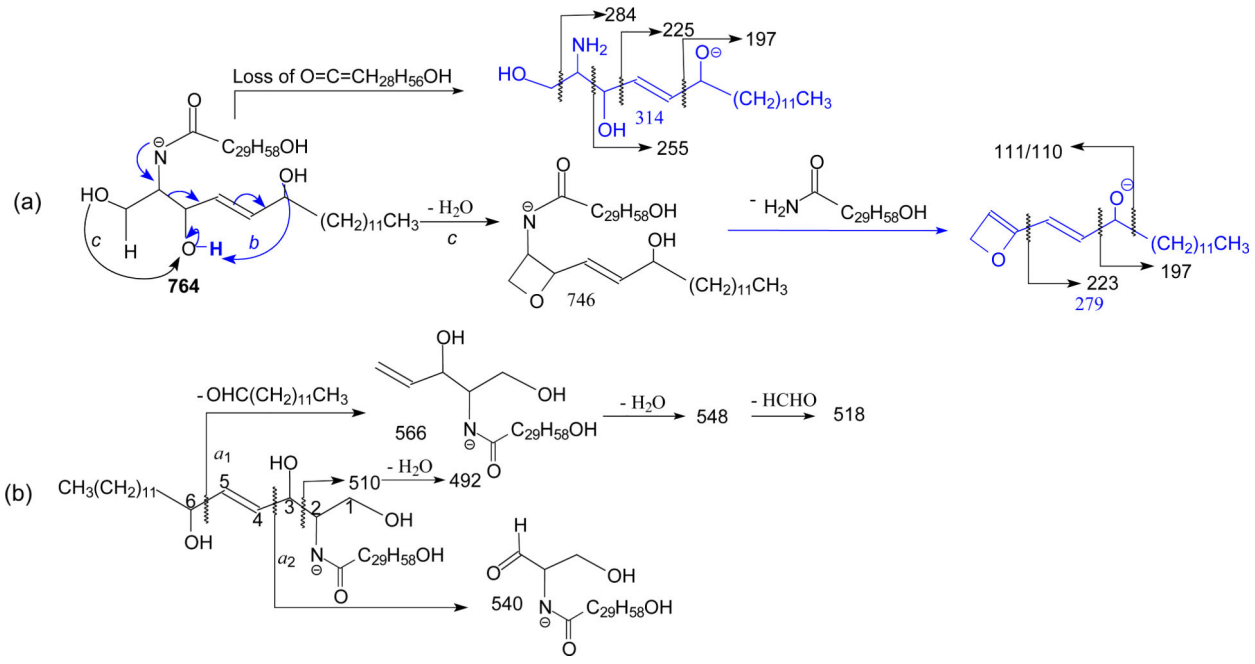

Scheme 8.

Table 1

The LIT MS^2 spectra of the $[M - H]^-$ ions of various ceramides included in the study ([1]Ceramide type abbreviation is according to references (27, 30); Rel. Intensity (%) in parenthesis; *overlapped m/z)

				common ions						FA related ions										LCB related ions							
A				c1	c2	c3	c4	c5	c6	a1	a2	a3	a4	a5	a6	a7	a8	a9	a10	d_{b1}	b2	b3	b4	b5	b6	b7	b8
$[M - H]^-$	LCB	FA	[1]Cer type	$[A\text{-}H_2O]^-$	$[A\text{-}H_2CO]^-$	$[A\text{-}H_2\text{-}H_2CO$	$c1\text{-}H_2O$	$[c1\text{-}H_2CO]^-$	$c5\text{-}H_2O$	[NAE-H]b	$a1\text{-}H_2$	$a1\text{-}H_2O$	$a2\text{-}H_2O$	$[a3\text{-}H_2O]^-$	RCO_2^-	$RCONH^-$	$RCO_2^-\text{-}H_2O$	$RCO_2^-\text{-}H_2 - CO_2$	$RCONH^- + 56$	[LCB-H]−	$b1\text{-}H_2CO$	$b1\text{-}H_2\text{-}H_2CO$	$c1\text{-}R_1CONH_2$	A - NAE	$c3\text{-}R_1CONH_2$	LCB + 41	b1 +CO
788	d17:1	ωh34:1	OS	770 (6.0)	758 (40)	756 (20)	752 (5)	740 (100)		564 (2.6)	562 (6.0)	546 (42.2)	544 (19.4)		521 (21.3)	520 (17.0)	503 (3.4)			284 (-)	254 (1.2)	252 (-)	249 (2.4)	223 (-)			
776	d18:1	ωh32:0	OS	758 (3.1)	746 (43.8)	744 (22.0)	740 (5.3)	728 (100)		536 (4.6)	534 (3.7)	520 (40.7)	518 (24.0)		495 (20.3)	494 (15.1)	477 (3.5)			298 (0.5)	268 (1.3)	266 (0.6)	263 (3.1)	237 (0.4)			
792	t20:1	ωh30:0	OH	774 (6.2)	762 (100)	760 (1.8)	756 (2.2)	744 (22.8)		510 (1.4)	508 (1.0)	492 (8.6)	490 (2.3)		467 (4.3)	466 (2.6)	449 (0.5)			342 (0.6)	312 (0.5)		307 (1.1)				
764	t18:1	ωh30:0	OH	746 (5.6)	734 (100)	732 (0.9)	728 (1.4)	716 (22.5)		510 (1.5)	508 (0.9)	492 (11.8)	490 (3.1)		467 (5.5)	466 (3.6)	449 (0.5)			314 (0.5)	284 (0.6)		279 (1.1)	253 (0.5)			
708	t18:1	αh26:0	AH	690 (25.7)	678 (100)	676 4.5)	672 (8.3)	660 (10.2)		454 (5.4)	452 (5.9)	436 (10.5)			411 (28.9)	410 (14.1)	393 (5.1)	365 (10.6)	466 (1.3)	314 (4)	284 (5.7)		279 (2.2)	253 (0.8)			
680	t18:1	αh24:0	AH	662 (25.2)	650 (100)	648 (8.7)	644 (10.2)	632 (9.8)		426(6.3)	424 (7.6)	408 (11.4)			383 (35.6)	382 (15.5)	365 (6.8)	337 (12.2)	438 (3.2)	314 (4.7)	284 (7.5)		279 (2.7)	253 (1.3)			
692	d18:1	βh26:0	BS	674 (3.2)	662 (2.2)	660 (0.9)	656 (0.3)	644 (1.2)				436 (0.3)								298 (0.6)	268 (2.4)	266 (0.9)	263 (4.9)	237 (2.1)		340 (100)	
678	d17:1	βh26:0	BS	660 (3.5)	648 (1.7)	646 (1.4)	642 (0.3)	630 (1.3)				436 (0.2)								298 (0.7)	254 (2.6)	252 (1.0)	249 (4.6)	223 (1.8)		326 (100)	
664	d18:1	αh24:0	AS	646 (43.3)	634 (9.0)	632 (10.5)	628 (8.6)	616 (100)		426 (3.6)	424 (40.8)	408 (18.3)		390 (2.8)	383 (9.8)	382 (3.4)	365 (5.7)	337 (23.4)		298 (3.1)	268 (9.4)	266 (0.7)	263 (1.3)	237 (0.7)			
580	d18:1	αh18:0	AS	562 (22.9)	550 (5.1)	548 (6.6)	544 (6.7)	532 (100)		342 (1.8)	340 (26.1)	324 (11.7)		306 (1.3)	299 (15.2)	298 (8.2)	281 (5.9)	253 (15.5)		298 (8.2)	268 (9.1)	266 (0.6)	263 (1.5)	237 (0.7)			
552	d18:1	αh16:0	AS	534 (36.0)	522 (6.0)	520 (7.8)	516 (7.4)	504 (100)		314 (0.9)	312 (35.6)	296 (17.2)		278 (2.8)	271 (13.6)	270 (0.7)	253 (5.0)	225 (9.1)		298 (7.5)	268 (2.8)	266 (0.5)	263(1.5)	237 (0.5)			
538	d17:1	αh16:0	AS	520 (33.1)	508 (5.6)	506 (8.0)	502 (6.0)	490 (100)		314 (0.9)	312 (26.1)	296 (14.9)		278 (2.0)	271 (10.6)	270 (3.0)	253 (1.1)	225 (12.0)		284 (6.1)	254 (3.1)	252 (-)	249 (0.6)	223 (1.2)			
650	d18:0	24:0	NdS	632 (12.6)		618 (100)	614 (1.0)	602 (46.6)		410 (2.7)	408 (33.5)	392 (90.4)			367 (34.6)	366 (5.7)	349 (18.2)			300 (8.0)		268 (1.4)		239 (2.2)			
566	d18:0	18:0	NdS	548 (16.0)		534 (100)	530 (2.6)	518 (60.1)		326 (2.1)	324 (27.0)	308 (92.7)			283 (32.0)	282 (7.7)	265 (18.8)			300 (11.4)		268 (3.7)		239 (5.5)			
648	d18:1	24:0	NS	630 (8.0)	618 (100)	616 (42.6)	612 (0.6)	600 (17.0)		410 (0.6)	408 (21.9)	392 (85.7)			367 (39.3)	366 (35.3)	349 (16.0)			298 (2.1)	268 (2.3)	266 (0.6)	263 (19.8)	237 (5.5)			
646	d18:1	24:1	NS	628 (5.6)	616 (100)	614 (39.6)	610 (0.4)	598 (13.0)		408 (0.4)	406 (20.4)	390 (93.4)			365 (12.5)	364 (9.8)	347 (9.6)			298 (2.2)	268 (0.9)	266 (0.3)	263 (15.1)	237 (4.5)			
564	d18:1	18:0	NS	546 (8.5)	534 (100)	532 (44.1)	528 (0.9)	516 (17.7)		326 (0.8)	324 (18.2)	308 (70.9)			283 (28.8)	282 (25.6)	265 (12.4)			298 (3.7)	268 (3.5)	266 (0.8)	263 (29.8)	237 (9.0)			
562	d18:1	18:1	NS	544 (5.7)	532 (100)	530 (40.6)	526 (0.5)	514 (15.7)		324 (0.4)	322 (18.4)	306 (81.5)			281 (33.5)	280 (19.2)	*263 (38.4)			298 (3.6)	268 (3.7)	266 (0.9)	263 (38.4)	237 (9.9)			
536	d18:1	16:0	NS	518 (7.4)	506 (100)	504 (43.7)	500 (1.0)	488 (36.2)		298 (3.6)	296 (18.7)	280 (72.8)			255 (22.6)	254 (22.0)	237 (23.7)			298 (3.6)	268 (4.5)	266 (1.0)	263 (32.0)	*237 (23.7)			
536	d16:1	18:0	NS	518 (5.3)	506 (100)	504 (36.7)	500 (-)	488 (13.3)		326 (-)	324 (24.5)	308 (82.6)			283 (40.0)	282 (35.5)	265 (6.4)			270 (1.5)	240 (3.3)	238 (0.7)	235 (30.1)	209 (6.3)			
626	t18:0	αh20:0	AP	608 (18.0)	596 (1.7)	594 (10.4)	590 (8.1)	578 (1.1)		370 (25.5)	368 (1.7)	352 (2.4)		334 (1.8)	327 (100)	326 (8.8)	309 (2.7)	*281 (22.5)	382 (34.8)	316 (1.5)		284 (1.7)	*281 (22.4)	255 (3.6)	267 (6.3)		
612	t17:0	αh20:0	AP	594 (19.6)	582 (1.9)	580 (10.5)	576 (10.2)	564 (1.6)		370 (29.5)	368 (3.7)	352 (2.7)		334 (1.8)	327 (100)	326 (10.0)	309 (3.2)	281 (21.5)	382 (36.8)	302 (1.6)		270 (1.6)	267 (1.2)	241 (2.9)	253 (6.4)		
598	t16:0	αh20:0	AP	580 (16.6)	568 (1.2)	566 (9.0)	562 (8.0)	550 (1.1)		370 (30.0)	368 (2.5)	352 (2.0)		334 (1.9)	327 (100)	326 (11.2)	309 (2.5)	281 (18.0)	382 (34.8)	288 (1.2)		256 (1.3)	253 (1.4)	227 (2.3)	239 (4.9)		
570	t18:0	αh16:0	AP	552 (17.6)	540 (0.9)	538 (8.9)	534 (8.6)	522 (1.1)		314 (31.2)	312 (2.0)	296 (1.5)		278 (1.2)	271 (100)	270 (10.6)	253 (3.6)	225 (23.3)	326 (44.4)	316 (1.9)		284 (2.0)	281 (1.8)	255 (7.2)	267 (15.9)		
556	t17:0	αh16:0	AP	538 (23.0)	526 (1.1)	524 (10.6)	520 (8.3)	508 (1.6)		314 (32.1)	312 (4.0)	296 2.2)		278 (1.2)	271 (100)	270 (11.6)	253 (2.6)	225 (26.3)	326 42.4)	302 (1.8)		*270 (11.6)	267 (1.5)	241 (5.1)	253 (9.1)		
610	t18:0	20:0	NP	592 (27.7)	580 (2.9)	578 (34.3)	574 (38.7)	562 (2.8)		354 (64.9)	352 (13.0)	336 (3.8)			311 (78.4)	310 (8.7)	293 (1.6)		366 (100)	316 (1.8)		284 (1.2)	281 (2.4)	255 (3.3)	267 (48.7)		
554	t16:0	18:0	NP	536 (14.1)	524 (2.0)	522 (13.0)	518 (20.3)	506 (0.8)		326 (58.1)	324 (8.0)	308 (2.0)			283 (100)	282 (4.0)	265 (0.3)		338 (87.0)	288 (1.0)		256 (0.6)	253 (-)	227 (2.2)	239 (43.0)		
554	t18:0	16:0	NP	536 (37.1)	524 (2.5)	522 (46.5)	518 (42.8)	506 (3.5)		298 (63.6)	296 (14.9)	280 (4.3)			255 (74.3)	254 (7.2)	237 (1.1)		310 (100)	316 (4.1)		284 (2.3)	281 (1.4)	*255 (74.3)	267 (62.7)		
554	d18:0	αh16:0	AdS	536 (100)	524 (1.6)	522 (40.9)	518 (7.5)	506 (22.2)	488 (16.8)	314 (3.5)	312 (8.8)	296 (32.3)			271 (34.8)	270 (2.0)	253 (15.0)	225 (29.2)		300 (80.0)		268 (20.7)	265 (3.0)	239 (13.0)			328 (5.8)
540	d17:0	αh16:0	AdS	522 (100)	510 (2.8)	508 (41.9)	504 (7.6)	492 (31.2)	474 (14.1)	314 (9.0)	312 (8.4)	296 (28.4)			271 (32.3)	270 (3.8)	253 (13.2)	225 (34.5)		286 (63.9)		254 (20.1)	251 (2.5)	225 (34.5)			314 (9.0)
526	d18:0	αh14:0	AdS	508 (100)	496 (1.2)	494 (40.8)	490 (5.0)	478 (13.0)	460 (32.4)	286 (3.5)	284 (7.8)	268 (60.5)			243 (30.1)	242 (2.8)	225 (12.4)	197 (24.8)		300 (85.3)		268 (60.5)	265 (3.5)	239 (15.0)			328 (4.4)